HYDROGEN PRODUCTION BY CATALYTIC METHANE DECOMPOSITION OVER RICE HUSK DERIVED SILICA

G. Gómez-Pozuelo[a], P. Pizarro[a,b], J.A. Botas[a], D.P. Serrano*[a,b]

[a] Chemical and Environmental Engineering Group, ESCET, Rey Juan Carlos University, 28933 Móstoles, Madrid, Spain

[b] Thermochemical Processes Unit, IMDEA Energy, 28935 Móstoles, Madrid, Spain

Abstract

Methane decomposition ($DeCH_4$) over solid catalysts is an interesting route for the production of hydrogen free of CO_2 emissions. Moreover, it could lead to a negative carbon balance if biogas/biomethane is used as feedstock. However, it is limited by the huge amounts of carbon that are deposited over the catalyst causing its deactivation and hindering its regeneration, which makes necessary the development of low-cost and durable catalytic systems. This work reports the use of different silica materials fully produced from rice husk, i.e. without incorporating any external phase or component, as $DeCH_4$ catalysts. The highest catalytic activity has been found for the silica samples showing large BET surface area and amorphous nature. These properties favor the generation of the actual $DeCH_4$ active sites (-Si-C- species), shortening the induction time detected at the beginning of the reaction tests. The nano-silica materials produced from acid-washed rice husk exhibit a remarkable resistance against deactivation, affording an almost constant hydrogen production during at least 12 h of time of stream. This fact is assigned to the presence of large mesopores that facilitate the growth of the carbons deposits towards the outer part of the catalyst particles. The results here reported show the great potential of rice husk derived nano-silica to overcome several of the most relevant limitations that currently exist for the commercial deployment of hydrogen production by catalytic $DeCH_4$, as a consequence of the low cost and durable activity of these sustainable materials.

Keywords: rice husk, nano-silica, hydrogen production, methane decomposition

1. Introduction

Hydrogen is a clean energy carrier whose combustion results only in the formation of water, thus avoiding the production of CO_x and other contaminants and pollutants [1]. However, hydrogen cannot be found in a free state in our planet, so it must be produced from other compounds (such as, hydrocarbons, biomass, and water), which requires the external supply of energy. Therefore, the consideration of hydrogen as a sustainable and clean fuel depends on both the raw material and the energy source employed for its generation. Currently, the principal route for hydrogen production at large scale is steam reforming of methane (SRM), which involves significant CO_2 emissions. A possible solution to this hindrance is the capture and storage of the produced CO_2, although it increases the price of the process and reduces its efficiency [2].

An attractive alternative to produce hydrogen is the decomposition of methane ($DeCH_4$) according to the following reaction [3–5]:

$$CH_4\,(g) \rightarrow C\,(s) + 2H_2\,(g) \qquad \Delta H^{\circ} = 75.6\ kJ \cdot mol^{-1} \qquad (1)$$

As in this process carbon is extracted from methane in solid form, it is possible to produce H_2 with high purity and without greenhouse gases (GHG) emissions. In addition, a variety of applications have been proposed for the carbonaceous product, including soil amendment, building and construction material and the manufacture of nanostructured carbonaceous solids, such as carbon nanotubes and nanofibers, with advanced properties. Likewise, an important point to be considered in terms of sustainability is the possibility of using biogas or biomethane as feedstock in the $DeCH_4$ process, which in turn could afford a negative CO_2 balance. This alternative is one of the few routes for hydrogen production showing a net carbon fixation effect [3,4].

Methane decomposition ($DeCH_4$) is an endothermic reaction having a lower enthalpy per mol of hydrogen than SRM (37.8 and 69 $kJ \cdot mol^{-1}$, respectively). However, methane is a relatively stable molecule and its thermal decomposition requires reaching elevated temperatures (at least 1,200 ºC). An effective route to decrease the reaction temperature is the use of metals and carbon based catalysts [6,7].

The metals showing the most relevant catalytic properties for methane decomposition are those of group VIII, mainly Ni, Ni/Cu, Fe and Co, which exhibit high activity at moderate reaction temperatures. These active phases are typically supported on metal oxides, such as Al_2O_3, SiO_2, MgO, TiO_2 and La_2O_3, or carbon materials, hence the effect of the support on methane decomposition must be considered. In the case of the Ni based catalysts, the carbon is often produced in the form of nanotubes, which significantly increases the value of this product [8–12]. Addition of noble metals into this type of catalysts has been reported to improve the activity and stability, but their high cost limits the industrial application of these systems for methane decomposition [13].

Carbonaceous materials have been also widely studied as catalysts [14,15], including carbon blacks [16], activated carbons [17,18], ordered mesoporous carbons [19–22], carbide-derived carbons (DTU-19) [23], hierarchical porous carbons [24], and metal/cellulose derived carbon [25]. In particular, ordered mesoporous carbons (CMK-3 and CMK-5) have shown excellent catalytic behavior and stability in hydrogen production by $DeCH_4$ [19–22]. However, these mesostructured carbons are prepared by nanocasting techniques, which makes very difficult the scaling up of the synthesis recipes for their commercial manufacture.

Interestingly, pioneering studies on methane decomposition (published in 1916, 1929 and 1931) reported the occurrence of this reaction also over silica surfaces, although no clear conclusions were disclosed on the possible effect of those silica materials on the methane conversion and the reaction rate [26–28]. Thereafter, and for many decades, the major use of silica in methane decomposition was as support of metallic phases. Just very recently, our research group reported the catalytic behavior in the $DeCH_4$ process of a variety of pure silica materials, having different textural and crystalline properties, such as zeolites and ordered mesoporous MCM-41 and SBA-15 [29,30].

One of the major hindrances in catalytic methane decomposition is the catalyst deactivation due to the deposition of large amounts of carbon. Despite formation of carbon cannot be avoided in this process, being one of the two products obtained in the reaction, it is possible to attenuate its deactivating effect by a right selection of the catalyst porosity and textural properties. Moreover, regeneration of the catalysts in this system is not straightforward since it would require the combustion of the carbon

deposits, provoking the formation of CO_2 and the loss of the major environmental advantages of $DeCH_4$ in comparison with other routes like SRM. Therefore, the development of low-cost materials with relevant catalytic activity in methane decomposition is an essential aspect for the commercial deployment of this process. Yang et al. [31] have recently reported the use of natural sand, formed mainly by silica, as a non-conventional catalyst for methane decomposition operating at temperatures between 850 and 950 ºC, although exhibiting low methane conversion due to the low BET surface of the used sand (below 1 m^2/g).

Silica is present in plant biomass as phytoliths, which are rigid microscopic structures with varying shapes and sizes. The silica content in plants depends largely on the specie, being mainly in the form of amorphous hydrated silica. In the case of rice husk the silica content can be as high as 20 wt.%. Moreover, since the disposal and management of rice husk residues is an important environmental problem, different methods have been developed for its valorization through the production of silica materials. Depending on the final properties, this silica can be used in multiple applications, like the preparation of zeolites, solar cells, sorbents and as catalyst for the synthesis of biofuel additives [32–35].

Regarding hydrogen production by $DeCH_4$, just two works can be found so far in the literature dealing with the use of rice husk-derived silica for the formulation of the catalysts [36,37]. In both cases, the catalysts include other components in addition to silica from rice husk, the latter being used mainly as a support rather than active phases of this reaction. Thus, rice husk-derived silica was modified by incorporation of both Pd and CeO_2 so the final composition of the catalyst was 0.7 wt.% Pd, 32 wt.% Ce and 18 wt.% Si [36]. Likewise, in other work [37], rice husk-derived silica was first modified by wet impregnation (1:1 weight ratio) of Al_2O_3, CeO_2, La_2O_3 and MgO, respectively, the resulting binary oxides were subsequently modified by impregnation with 50 wt.% of Ni that was the actual active phase for the $DeCH_4$ reaction.

In this context, the present work discloses for the first time the catalytic properties of silica materials fully prepared from rice husk, without adding any external metallic phase, in hydrogen production by methane decomposition. The results here reported indicate that tailoring the textural and structural

properties of the rice husk derived silica affords the development of low-cost and sustainable catalysts with significant activity and strong resistance against deactivation in methane decomposition, overcoming some of the major limitations that hinder the commercial deployment of this process for the production of hydrogen free of CO_2 emissions.

2. Experimental

2.1. Preparation of rice husk derived-silica samples

The rice husk employed in this research was obtained from a rice mill located in Huesca province (Spain), being supplied by Avidem company. Initially, the raw rice husk was washed with water and dried in an oven at 100 ºC during 3 - 4 h. The dried sample was pulverized in a RETSCH Ultra Centrifugal Mill ZM100 to get a powder and, then, it was screened through ASTM standard sieves to obtain the desired grain sizes: RH≤100 and 100≤RH≤250 μm (rh/100 and rh/250 materials, respectively). In order to remove mineral matter, a portion of both sieved samples was treated with 1 M HNO_3 (Scharlab, 60 wt.%) solution at 60 ºC for two hours. Subsequently, the de-ashed solids were washed until neutral pH and dried, being named as as aw-rh/100 and aw-rh/250.

The different rice husk powders were subjected to slow pyrolysis at 400 ºC, with a heating rate of 2 $ºC \cdot min^{-1}$, under nitrogen atmosphere using a tubular furnace to produce the corresponding rice husk derived-char samples: char/100, char/250, aw-char/100 and aw-char/250. Finally, silica-based materials were obtained through the combustion of these chars by heating at 5 $ºC \cdot min^{-1}$ until 700 ºC under 100 $ml \cdot min^{-1}$ of air. The rice husk derived-silica samples were named as: SiO_2/100, SiO_2/250, aw-SiO_2/100 and aw-SiO_2/250.

2.2. Materials characterization

Both raw and acid-treated rice husk samples were characterised following UNE-EN 14774-1:2010, UNE-EN 14775:2010 and UNE-EN 15148:2010 to obtain the moisture, ash and volatile matter contents, respectively. Moisture content was determined by the sample weight loss after oven treatment at 105 ºC during 3 h. On the other hand, the ash content was obtained calculating the total weight loss after

calcination of the dry biomass at 550 ºC for 3 h under static air. Thermogravimetric analyses were carried out in a simultaneous TGA-DSC1 thermobalance (Mettler Toledo) to calculate the volatile matter. In this way, the dried biomass was heated up to 900 ºC under inert conditions (N_2, 100 $cm^3 \cdot min^{-1}$), assigning the weight loss to volatile matter. Finally, the fixed carbon was calculated according to the next equation:

$$\text{Fixed carbon (wt.\%)} = 100 - \text{volatile matter (wt.\%)} - \text{Ash (wt.\%)} \quad (2)$$

The elemental composition (CHN/O) of the rice husk samples was determined using a Thermo Fisher Scientific Flash 2000 Elementar Analyzer. The chemical composition of rice husk ash (mineral matter) was measured by inductively coupled plasma-optical emission spectroscopy (ICP-OES) with a Perkin Elmer Optima 3000 DV instrument. Prior to the analyses, the ash was collected by burning 20 g of both raw and acid-washed rice husk in a muffle oven at 900 ºC under air atmosphere. Then, a representative amount of sample was digested by treatment with a mixture of HF and HNO_3 in an Anton Paar (MW3000) microwave equipment.

The textural properties of rice husk derived-silica samples were determined from N_2 adsorption-desorption isotherms at 77 K using a Micromeritics Tristar 3000 analyser. Previously to the tests, the samples were outgassed for 8 h under vacuum at 200 ºC. The Brunauer-Emmer-Teller (BET) equation was used to calculate the surface area in the relative pressure range between 0.05 and 0.2. The total pore volume was measured at a relative pressure of 0.98. The rice husk samples, the char obtained after their pyrolysis and the derived-silica materials were characterized by X-ray diffraction (XRD), using a Philips X'Pert MPD/MRD diffractometer with Cu Kα monochromatic radiation in the range of 10 – 50º. Transmission Electron Microscopy (TEM) images were taken in a Philips Technai 20 and JEOL JEM 2100 microscopes, operating with a tungsten filament working at 200 kV.

The thermal behaviour of both rice husk and char samples was evaluated by means of thermogravimetric analysis in nitrogen and air, respectively, using a simultaneous TGA-DSC1 thermobalance (Mettler Toledo). The conditions employed in these tests were the same as those applied for the pyrolysis and combustion treatments above described (section 2.1) for the preparation of the rice husk silica samples.

2.3. CH_4 decomposition experiments

The activity of rice husk derived-silica materials in $DeCH_4$ was investigated using a simultaneous DSC-TGA thermobalance (TGA-DCS1, Mettler Toledo). Typically, a flow of 200 ml·min^{-1} of 10% CH_4 in argon was employed as reactive gas. The sample holder was an alumina crucible with a volume of 150 µL. Reactions were operated under temperature-programmed and isothermal conditions. Prior to the tests, silica materials were dried at 250 ºC with nitrogen. For isothermal reaction tests, the dried samples were heated under 200 ml·min^{-1} of nitrogen flow until reaching the target temperature (890, 940, 965 and 990 ºC, respectively). Then, the reaction was initiated by feeding the methane/argon mixture with a flow rate of 200 ml·min^{-1}, recording the sample weight along the time on stream. In the case of temperature programmed tests, after drying, the samples were purged under the flow of the reaction mixture and the temperature was increased from 50 ºC to 1,100 ºC with a constant heating rate of 10 ºC·min^{-1}, being kept constant at 1,100 ºC for 60 min. Preliminary TG tests performed under inert atmosphere, i.e. in the absence of methane, showed the high thermal stability of the rice husk-derived silica as the weight of the samples remained practically constant when increasing the temperature over 700 ºC. The progress of methane decomposition was monitored through the weight increase of the silica sample due to the carbon deposition, according to the stoichiometry of the reaction (equation 1). A blank test was performed employing an empty crucible at the highest reaction temperature (1,100 ºC), confirming that the contribution of thermal decomposition of methane was almost negligible under the conditions employed in the TG tests.

3. Results and discussion

3.1 Properties of the rice husk derived-samples

The silica samples were obtained from rice husk following a two-step thermal treatment, as described in the experimental section. Thereby, the raw rice husk was first subjected to carbonization in inert atmosphere and then to air combustion in order to remove the organic matter. Moreover, with the aim to investigate the effect of the mineral matter contained in the rice husk, two samples were prepared by

applying an acid washing treatment before the carbonization step. Since the raw rice husk was grounded and sieved into two fractions, a total of four different silica samples were produced.

Table 1 shows the composition of both raw and acid-treated rice husk samples according to proximate and ultimate analyses. The fraction with the smallest grain size (rh/100) contains more mineral components (mainly silica) than the rh/250 sample (15.8 versus 9.7 wt.%, respectively) and presents lower volatile matter, fixed carbon and water [38]. The ash content is slightly reduced after the acid-washing treatment, this effect being more pronounced for the rice husk with the lowest grain size, which is compensated by an increase in the fixed carbon. Regarding the elemental compositions, both fractions show relatively similar compositions, with oxygen and carbon contents typical of lignocellulose in the range of 47.0–48.2 and 45.4–47.6 wt.%, respectively [39], whereas the H content is about 5-6 wt.% for all the samples.

The concentration of other metallic elements, different from Si, in the different samples was determined by ICP-OES. As illustrated in Figure 1, the rice husk samples contain Na, Al, Ca, Fe, K, Mg and P as the major inorganic components. Significantly higher contents are present in the raw rice husk with the smallest particle size. It is observed that, although not completely, the acid-washing treatment is effective in removing a great part of those elements. Similar results are shown in Table 2 for the final silica samples. Comparing the two samples prepared omitting the acid treatment, it is observed that the highest concentration of the metal oxides corresponds to SiO_2/100, i.e. the sample having the lowest particle size, which is consistent with its also higher ash content. As expected, the acid-washed silica samples present metal contents clearly lower than the corresponding untreated ones. Thus, Mg, P and K are detected in very small amounts for the silica materials prepared including the acid-washing treatment. Significant reductions are also observed for Fe and Ca oxides, whereas Al and Na seem to be more refractory to the acid-washing treatment, keeping significant contents of these metals, especially in the case of the silica sample with larger particle size.

Table 1. Proximate and ultimate analyses of raw and acid-washed rice husk samples.

	Proximate Analyses (wt.%)				Ultimate Analyses[c] (wt.%)			
Sample	**Ash[a]**	**Volatile matter[a]**	**Fixed Carbon[a,b]**	**Moisture**	**C**	**H**	**N**	**O**
rh/100	15.8	66.5	17.7	3.5	48.2	6.0	0.4	45.4
rh/250	9.7	68.9	21.4	4.1	47.8	5.2	0.2	46.8
aw-rh/100	14.4	66.4	19.2	2.8	47.0	5.0	0.4	47.6
aw-rh/250	9.5	68.8	21.7	3.0	47.6	5.7	0.2	46.5

[a] Dry basis; [b] determined by difference; [c] calculated on dry and ash free basis

Table 2. Composition of the silica samples obtained from both raw and acid-washed rice husk, expressed as the corresponding oxides (wt.%).

Sample	**Al_2O_3**	**BaO**	**CaO**	**Fe_2O_3**	**K_2O**	**MgO**	**MnO**	**Na_2O**	**P_2O_5**	**SnO_2**	**SrO**	**TiO_2**	**SiO_2**
SiO_2/100	2.46	0.01	2.22	1.99	0.95	0.70	0.08	5.14	0.50	0.01	0.01	0.02	85.9
SiO_2/250	1.83	0.01	1.80	0.71	0.55	0.65	0.01	4.19	0.30	0.01	0.01	0.02	89.9
aw-SiO_2/100	1.70	0.01	0.74	0.23	0.05	0.02	0.01	3.59	0.09	0.01	0.01	0.02	93.5
aw- SiO_2/250	0.40	0.01	0.04	0.18	0.01	0.02	0.01	3.87	0.07	0.01	0.01	0.02	95.4

Figures 2(a) and (b) show the TG/DTG curves obtained under nitrogen atmosphere for the four rice husk samples. A progressive weight loss starting at about 170 ºC is observed corresponding to the decomposition of the organic components (mainly holocellulose) [32,40,41]. Despite overlapped, two signals can be appreciated in the DTG curves. The first one occurs as a shoulder at about 250 - 260 ºC and is originated by the decomposition of hemicellulose, while the second peak, centred at about 290 ºC, can be attributed to the degradation of cellulose [42]. Lignin undergoes a more gradual decomposition along the temperature range, being also the main responsible of char formation [32,40]. On the other hand, the two samples subjected to acid-washing exhibit a decrease in the intensity on the first peak at expense of a higher intensity on the second one, suggesting that a partial degradation of hemicellulose takes place during the acid treatment. Nevertheless, the removal of alkaline and alkaline earth metals during the acid-washing, which are known to catalyse the decomposition of cellulose and hemicellulose [43], may have also an effect on the changes observed in the low-temperature DTG peak. Regarding the particle size of the rice husk samples, no significant variations in the decomposition temperatures are observed, whereas slightly larger residue weights at the end of the TG experiments are observed for the samples with the smallest dimensions, being in line with their higher ash content.

Figures 2(c) and (d) illustrate the TG/DTG curves under air atmosphere of the rice husk derived-chars, which provides information about the combustion process of the carbonaceous material they contain. For each sample, a major peak is observed in the DTG curve with a minor shoulder contribution at lower temperatures. These two steps can be related with the combustion of the softer fraction of char, comprising smaller compounds and oligomers, and of fixed carbon or harder char, respectively [41,44]. In the case of char/100 and char/250 the peak maxima corresponding to these two steps are located at about 350 ºC and 445 ºC, respectively. In contrast, these signals are clearly shifted towards higher temperatures (c.a. 385 ºC and 490 ºC, respectively) in the case of the chars obtained from the acid-washed rice husk samples. This finding denotes that the conversion of the char is favoured for the non-acid treated samples, which may be explained by their higher content in metallic species as they can catalyse the combustion process [45]. The residual weight in the air-TG tests is directly linked to the ash content of the char samples.

Figure 3(a) displays the nitrogen adsorption-desorption isotherms at 77 K for the four silica materials prepared from rice husk, whereas the resulting textural properties are summarized in Table 3. Huge differences are observed between the adsorption-desorption isotherms of these samples, denoting the strong effect of the silica preparation method. Thus, the silica materials derived from untreated rice husk (SiO_2/100 and SiO_2/250) present little N_2 uptake, which indicates relatively weak adsorption forces between adsorbate and adsorbent [46] and the almost total absence of both micro- and mesopores. This is also reflected in the low BET surface area of these samples (9 and 30 $m^2\ g^{-1}$). In contrast, the silica samples prepared from acid-treated rice husk (aw-SiO_2/100 and aw-SiO_2/250) present significant N_2 adsorption, showing a mix of type II and IV(a) isotherms with an H4 hysteresis loop [47]. Accordingly, these silica materials possess rather larger textural properties in comparison with those derived from non-acid washed rice husk. In particular, the highest BET surface (280 $m^2 \cdot g^{-1}$) and pore volume (0.36 $cm^3 \cdot g^{-1}$) correspond to the silica prepared from de-ashed rice husk with the lowest particle size (aw-SiO_2/100). As it is illustrated in Figure 3(b), silica samples derived from acid-washed rice husk contain a significant proportion of mesoporosity with a relatively broad mesopore size distribution (peak maxima at about 7 nm). In the case of aw-SiO_2/250 the porosity is extended even up to the macropore

range. In contrast, application of the t-plot method evidences the absence of micropores for all samples. Interestingly, the N_2 uptakes for both series of samples (acid-washed and untreated ones) are larger in the case of the silica materials derived from the rice husk fraction with the smallest particle size, evidencing a direct relationship between the textural properties and the grain size in the raw biomass.

Table 3. Textural properties of rice husk derived-silica samples.

Sample	**SiO_2/100**	**SiO_2/250**	**aw-SiO_2/100**	**aw-SiO_2/250**
S_{BET} ($m^2 \cdot g^{-1}$)	30	9	280	153
V_{pore} ($cm^3 \cdot g^{-1}$)	0.11	0.004	0.36	0.27

Figure 4(a) illustrates the XRD patterns of raw and acid-treated rice husk samples. All of them present similar diffraction patterns with peaks located at 2θ = 16º, 23º and 34º, typical of cellulose [48–50]. This biopolymer has crystalline structure due to hydrogen bonding interactions and Van der Waals forces between adjacent molecules, contrary to hemicellulose and lignin, which are amorphous. After carbonization, the so obtained rice husk derived-chars exhibit the XRD patterns shown in Figure 4(b). A broad signal can be observed at about 2θ = 23º corresponding to the (002) reflection of amorphous silica [42].

Sharp differences are detected between the final silica samples regarding their crystalline properties, as illustrated in the XRD patterns of Figure 4(c). Thus, clear crystalline fringes are observed in both silica samples obtained from untreated rice husk, i.e. with a higher content of mineral components, while they are absent (or present with very small intensity) in the XRD of the silica materials derived from acid-washed rice husk. Thus, the XRD pattern of SiO_2/250 corresponds to a highly crystalline silica, having contributions of different phases: cristobalite, which seems to be the predominant one, tridymite and quartz. The theoretical sequence of the thermal conversion of silica is α-quartz, β-quartz (573 ºC), β-tridymite (870 ºC) and β-cristobalite (1,470 ºC), but the presence of ions may lower the transition temperature between such phases [51,52]. In particular, alkali ions occupying interstitial sites of the silica may provoke the formation of crystalline phases during the thermal treatment [53]. This effect would explain the crystalline features of the silica samples with larger content of minerals.

On the other hand, the materials produced from acid-treated rice husk show mainly a broad XRD peak at 2θ = 22 º, indicative of essentially amorphous forms of silica. Nevertheless, two peaks corresponding to crystalline silica phases (quartz/tridymite) are appreciated for aw-SiO_2/250, despite this material reached a higher deashing than aw-SiO_2/100. This behaviour, together with the higher crystallinity degree of the untreated SiO_2/250 compared to that of SiO_2/100, evidences the remarkable effect of the rice husk particle size as an additional factor influencing the transition of silica from amorphous to crystalline phases. In this sense, it is concluded that larger particles undergo an enhanced densification/crystallization process during the rice husk combustion. These changes are in agreement with the textural properties of the samples as the formation of dense crystalline phases involves a strong reduction of both surface area and pore volume.

The morphology and nanoparticle size of acid-treated and untreated rice husk derived- silica samples with the lowest particle size (SiO_2/100 and aw-SiO_2/100, respectively) was investigated by transmission electron microscopy. As shown in Figures 5(a) and (b), both silica samples consist of a reticular network of interconnected/aggregated nanounits. The latter are clearly smaller for the de-ashed sample with sizes about 10 - 30 nm (aw-SiO_2/100) versus 50 - 100 nm (SiO_2/100). These findings are in agreement with the different textural properties corresponding to these samples, as above discussed, and in particular with the larger BET surface area of the aw-SiO_2/100 material.

3.2. DeCH_4 over rice husk derived-silica samples: temperature programmed reactions

The activity of the four silica samples for methane decomposition was first evaluated under temperature programmed conditions. Figure 6 illustrates the results of these tests in the form of weight increase of the catalyst sample, referred to the initial silica mass, due to the deposition of the carbon produced during the DeCH_4 reaction. For each sample, the threshold temperature (T_{th}) was calculated as the temperature at which a 0.05 % increase of the initial silica weight occurs [19]. The T_{th} values were always above 1,000 ºC, clearly higher than those obtained employing carbonaceous materials (700-800 ºC range) [21,22]. Interestingly, the derived-silica samples with large surface areas (aw-SiO_2/100 and aw-SiO_2/250) initiated the methane decomposition at lower temperatures and presented higher initial reaction rates (more pronounced slopes in the TG curves), leading to higher total carbon accumulations

and, accordingly, enhanced hydrogen productions. These materials contain amorphous walls with a high proportion of defective sites that are assumed to promote the formation of -Si-C- species, which in earlier works of our group have been proposed to be the actual active centers of methane decomposition, based on FTIR measurements [29,30]. In contrast, samples SiO_2/100 and SiO_2/250 show quite larger threshold temperatures (1,073 and 1,075 ºC, respectively) and lower initial reaction rates, as denoted by the smaller slope of the curves. Although these materials contain large amounts of ash and, therefore, of metallic species, that could act also as $DeCH_4$ catalysts, this fact does not seem to compensate their low surface area.

A few minutes after carbon deposition is started, an inflection point in the TG-curves occurred for the silica samples, especially for those obtained from acid-washed rice husk. The occurrence of this inflection point has been earlier observed when employing mesoporous materials as $DeCH_4$ catalysts, such as both ordered mesoporous carbons [19–22] and silicas [29,30], being assigned to the appearance of hindrances for the growth of the carbon deposits within the mesopores of the catalysts. This explanation agrees well with the features of the aw-SiO_2 samples, as they show a significant contribution of mesoporosity to the textural properties.

3.3. $DeCH_4$ over rice husk derived-silica samples: isothermal reactions

In our previous study comparing the behavior of different mesostructured silica SBA-15 materials in the $DeCH_4$ reaction, isothermal tests were carried out at 965 ºC [30]. The selection of this temperature ensured good activities while it avoided interferences from direct thermal decomposition of methane that could take place if higher temperatures were applied at long reaction times. Considering these premises, the four rice husk derived-silica samples were evaluated and compared under isothermal conditions at 965 ºC. The resulting cumulative carbon productions, referred to the initial mass of silica, are represented in Figure 7(a). Under these conditions, great differences were observed between the four silica samples, showing the following carbon formation order: SiO_2/250 < SiO_2/100 << aw-SiO_2/250 < aw-SiO_2/100. When no deashing treatment was applied, little $DeCH_4$ activity was attained in spite of the larger content of mineral components that could catalyze this reaction. Thus, the SiO_2/250 sample was practically inactive, whereas some initial carbon deposition was observed over SiO_2/100 but

with a very small slope and, therefore, low reaction rate beyond 2 h of time on stream. In contrast, the silica samples obtained from acid-washed rice husk exhibit significant activity in $DeCH_4$ reaction. These results confirm that the catalytic activity is mainly determined by the silica properties and not by the content of other inorganic components, such as Al-containing species that could impart some type of acidity to the silica materials.

It must be noted that, although the isothermal reactions have been performed at a temperature below the corresponding threshold temperatures, three of the silica samples exhibit significant catalytic activity. This apparent contradiction can be explained taking into account that the threshold temperatures have been determined from temperature programmed tests under dynamic (i.e. non-equilibrium) conditions. In this way, it is interesting to highlight that, during the isothermal experiments, carbon deposition was not detected at the beginning of the methane feeding into the thermobalance, but the existence of relatively long induction times, with values over 30 min, was observed. It could be thought initially that the existence of the induction time is provoked by a slow adsorption of the methane molecules on the catalyst surface. However, the values of the induction times (over 30 min) are too high for being assigned to methane adsorption as rate-controlling step. Conversely, this finding is in good agreements with the assumption that the real active sites catalyzing the methane decomposition are not present in the raw silica samples, but they are formed after a relatively long exposure to the methane atmosphere [29,30]. Similarly to the threshold temperature, the induction time was calculated as the time at which a 0.05 % increase of the initial silica weight takes place. As illustrated in Figure 7(b), an inverse relationship is observed between the values of the induction time and the BET surface of the samples, which agrees well with the increasing concentration of active site precursors (defective sites) expected in the materials with larger textural properties. Moreover, for the silica samples obtained from untreated rice husk and, in particular for the SiO_2/250 material, the increase in the induction time tends to be exponential, reaching values over 2 h. This result suggests that, in addition to its very small surface area, the high crystallinity of this silica sample prevents the formation of -Si-C- species.

Other remarkable finding from the results in Figure 7(a) is the high stability of the silica samples obtained from acid-washed rice rusk at long reaction times. Thus, the catalyst weight increase follows

an almost linear variation along the time, which means that the $DeCH_4$ reaction rate is practically constant with no signals of catalyst deactivation in spite of reaching high values of carbon deposition in respect to the initial silica mass. In this way, the amount of carbon deposited after 12 h was 0.83 and 0.42 $g_{Cdep} \cdot g_{silica}^{-1}$ for aw-SiO_2/100 and aw-SiO_2/250, respectively. This performance is better than that of other pure silica materials tested until now in this reaction [29], with the exception of SBA-15 that led to a carbon production of 2.29 $g_{Cdep} \cdot g_{silica}^{-1}$ when working at the same operation conditions. However, SBA-15 is a mesostructured silica produced by a time-consuming surfactant-assisted sol-gel procedure and using expensive reagents, hence this material would be a quite more expensive catalyst than the silica samples obtained from rice husk. Moreover, if the carbon production rate is referred to the BET surface of silica, almost the same value is obtained for both SBA-15 and aw-SiO_2/100, concretely $2.96 \cdot 10^{-3}$ and $3.0 \cdot 10^{-3}$ g_{Cdep}/m^2, respectively, denoting that the textural properties largely determine their catalytic activity for $DeCH_4$. This conclusion is also supported by the linear relationship existing between the carbon deposition at 12 h and the BET surface area of the different silica samples employed in the present work, as shown in Figure 7(c). Nevertheless, it must be taken into account that, as in the case of the induction time, the crystallinity of the silica materials obtained from untreated rice husk can also contribute to their low carbon formation rate due to a reduced concentration of defects and, therefore, of active sites.

Figure 8 illustrates TEM images of the aw-SiO_2/100 sample after being used in the $DeCH_4$ reaction. The presence of large amounts of carbonaceous material deposited over and embedding the silica can be observed in Figure 8(a). Moreover, it can be appreciated in Figure 8(b) that the carbon structures are able to grow towards the outer part of the silica particles, which would explain how the latter can keep a remarkable activity with the time without almost signals of deactivation.

3.4. Effect of temperature on $DeCH_4$ reaction over RH derived-silica samples

Due to their superior catalytic activity and stability along the reaction time of the silica materials obtained from acid-washed rice husk, they were selected for studying in deep the effect of the reaction temperature. Thereby, additional tests at 890, 940 and 990 ºC were carried out over these silica samples, the resultant TG curves being shown in Figures 9(a) and (b) for aw-SiO_2/100 and aw-SiO_2/250,

respectively. The superior catalytic activity of the aw-SiO_2/100 sample is denoted again at all the investigated temperatures in line with its larger surface area. As expected, for both silica materials, the rise of the temperature enhances the carbon formation as it increases the $DeCH_4$ reaction rate. Nevertheless, both materials present little activity at the lowest temperature (890 ºC). Then, the results obtained at this temperature have not been taken into account in the subsequent quantitative analysis.

The induction time is lower in all cases for the aw-SiO_2/100 sample, which can be also assigned to its larger BET surface in comparison with aw-SiO_2/250. For both materials, a strong effect of the temperature on the value of the induction time is appreciated. Thus, in the case of aw-SiO_2/100, the induction time is shortened from 192 min down to 14 min when increasing the temperature between 940 and 990 ºC. However, attempts to adjust the variation of the reverse of the induction time to Arrhenius type equations did not provide good fittings (Figure 10(a)), suggesting that the effect of the temperature on the generation of the actual active sites of $DeCH_4$ is a complex process involving different types of defective Si-O^- species, whose relative concentration on the silica surface may undergo significant variations with the temperature.

The presence of an inflection point is clearly observed for both silica samples in the curves of Figure 9, in special when operating at temperatures above 940 ºC. As a consequence, a maximum is present in the carbon deposition rates, calculated from the derivatives of the TG curves, along the time on stream in most of the experiments (see Figures 9© and 9(d)). This effect has been already observed in previous works using both carbon and pure silica materials as catalysts for $DeCH_4$ [29,30]. In the case of silica-based materials, such as those used in the current work, the initial increase in the reaction rate can be assigned to the progressive formation of the -Si-O^- sites that are the actual active centers of the reaction, although some influence of autocatalytic effects from the deposited carbons may also occur [20]. At longer times on stream, the overall kinetic regime of the process is modified due to the appearance of restrictions within the mesopores for the growth of the carbon deposits, provoking a drop of the reaction rate [19–21,29,30]. Nevertheless, it must be highlighted that the reaction rates reach a quasi-stationary state that last until the end of the assay, hence the rice husk derived silica keep a significant catalytic activity even after the formation of high amounts of carbon.

The superior performance of the aw-SiO_2/100 sample is also denoted in terms of carbon production at all temperatures compared to aw-SiO_2/250. Thus, at the highest temperature (990 ºC), the overall W_{Cdep}/W_{silica} ratio reaches values of 1.2 and 0.7 for aw-SiO_2/100 and aw-SiO_2/250, respectively, showing again the important effect of the surface area on the $DeCH_4$ catalytic activity. The carbon deposition rates at long times on stream showed reasonably good fittings with the temperature according to the Arrhenius equation, as shown in Figure 10(b). The values so obtained for the activation energy (167.4 and 225.9 kJ mol^{-1} for aw-SiO_2/100 and aw-SiO_2/250, respectively) can be compared with literature data. In this way, the activation energy of aw-SiO_2/250 is very close to that found for SBA-15 (217.8 kJ/ mol^{-1}) and agrees well with that corresponding to the crystalline carbon growth as the rate-limiting step (227.1 kJ/mol). Accordingly, the lower activation energy exhibited by aw-SiO_2/100 sample can be rationalized by its larger pore volume as it imposes lower restrictions for the outward growth of the carbon deposits.

In summary, all these results evidence the interesting catalytic properties of the silica materials prepared from acid-washed rice husk for hydrogen production by methane decomposition in terms of both catalytic activity and stability, pointing towards the textural properties as the main governing factors.

4. Conclusions

Hydrogen production by methane decomposition proceeds efficiently when using silica materials fully prepared from rice husk, i.e. without adding any external metal phase, as catalysts.

Both the grain size and acid-washing pre-treatment of the raw rice husk significantly influence the physico-chemical properties of the so obtained silica. Thus, untreated rice husk leads to poor BET surface area (9-30 $m^2 \cdot g^{-1}$) due to the catalytic effect of the mineral components during the combustion step, which promotes the formation of dense crystalline silica phases. On the contrary, combining acid washing with the use of small grain sizes (100 μm) leads to amorphous silica with relatively high surface area (280 $m^2 \cdot g^{-1}$) and pore volume (0.36 $cm^3 \cdot g^{-1}$).

During the $DeCH_4$ tests, the presence of an induction time was observed before the detection of the first catalytic activity. This delay is in agreement with the actual active sites being not present in the raw silica, but being created by reaction between defective sites in the silica surface and methane molecules to form -Si-C- species.

A number of silica properties have been identified as especially relevant in CH_4 decomposition: presence of amorphous silica walls, high surface area and large mesopores. In particular, a good correlation exists between two of the most important reaction parameters (induction time and reaction rate) with the catalyst BET surface area. Thus, the rice husk derived-silica obtained from the acid-washed biomass and with the smallest particle size exhibits the highest activity in $DeCH_4$, also showing a remarkable stability along the time on stream. This material consists of a reticular network of interconnected nanoparticles with sizes about 5 – 10 nm.

On the other hand, increasing the reaction temperature favours the generation of active sites, as denoted by the strong reduction in the induction time, and enhances the reaction rate.

These results pave the way for the development of sustainable and low-cost catalysts, based on rice husk derived nano-silica, exhibiting remarkable performance in methane decomposition for the production of hydrogen free of CO_2 emissions.

Acknowledgments

The authors gratefully acknowledge the financial support from the Spanish Ministry of Economy, Industry and Competitiveness and the Spanish State Research Agency through the project BIOCASCHEM (CTQ2017-87001-R) and from the Regional Government of Madrid through the project BIOTRES-CM (P2018/EMT-4344). We are also grateful to ICTS Centro Nacional de Microscopía Electrónica of the Universidad Complutense de Madrid (Spain) for the assistance with the TEM micrographs.

References

[1] Steinberg M. The Hy-C process (thermal decomposition of natural gas) potentially the lowest

cost source of hydrogen with the least CO_2 emission. Energy Convers Manag 1995;36:791–6.

[2] Scholz WH. Processes for industrial production of hydrogen and associated environmental effects. Gas Sep Purif 1993;7:131–9.

[3] Dufour J, Gálvez JL, Serrano DP, Moreno J, Martínez G. Life cycle assessment of hydrogen production by methane decomposition using carbonaceous catalysts. Int J Hydrogen Energy 2010;35:1205–12.

[4] Serrano DP, Dufour J, Iribarren D. On the feasibility of producing hydrogen with net carbon fixation by the decomposition of vegetable and microalgal oils. Energy Environ Sci 2012;5:6126–35. https://doi.org/10.1039/c2ee02709g.

[5] Keipi T, Tolvanen H, Konttinen J. Economic analysis of hydrogen production by methane thermal decomposition: Comparison to competing technologies. Energy Convers Manag 2018;159:264–73. https://doi.org/10.1016/J.ENCONMAN.2017.12.063.

[6] Alves L, Pereira V, Lagarteira T, Mendes A. Catalytic methane decomposition to boost the energy transition: Scientific and technological advancements. Renew Sustain Energy Rev 2020. https://doi.org/10.1016/j.rser.2020.110465.

[7] Abbas HF, Wan Daud WMA. Hydrogen production by methane decomposition: A review. Int J Hydrogen Energy 2010;35:1160–90.

[8] Piao L, Li Y, Chen J, Chang L, Lin JY. Methane decomposition to carbon nanotubes and hydrogen on an alumina supported nickel aerogel catalyst. Catal Today 2002;74:145–55. https://doi.org/10.1016/S0920-5861(01)00540-5.

[9] Reshetenko T V., Avdeeva LB, Khassin AA, Kustova GN, Ushakov VA, Moroz EM, et al. Coprecipitated iron-containing catalysts (Fe-Al_2O_3, Fe-Co-Al_2O_3, Fe-Ni-Al_2O_3) for methane decomposition at moderate temperatures I. Genesis of calcined and reduced catalysts. Appl Catal A Gen 2004;268:127–38. https://doi.org/10.1016/j.apcata.2004.03.045.

[10] Muradov NZ, Veziroğlu TN. From hydrocarbon to hydrogen-carbon to hydrogen economy. Int J Hydrogen Energy 2005;30:225–37. https://doi.org/10.1016/j.ijhydene.2004.03.033.

[11] Torres D, de Llobet S, Pinilla JL, Lázaro MJ, Suelves I, Moliner R. Hydrogen production by catalytic decomposition of methane using a Fe-based catalyst in a fluidized bed reactor. J Nat

Gas Chem 2012;21:367–73.

[12] Jyoti, Ashok CH, Srilatha K, Patil N, Shilpa Chakra CH. Hydrogen production from methane decomposition using nano metal oxides. Mater Today Proc 2017;4:11679–89. https://doi.org/10.1016/j.matpr.2017.09.082.

[13] Spiess FJ, Suib SL, Irie K, Hayashi Y, Matsumoto H. Metal effect and flow rate effect in the hydrogen production from methane. Catal. Today, 2004. https://doi.org/10.1016/j.cattod.2003.11.043.

[14] Zhang J, Li X, Chen H, Qi M, Zhang G, Hu H, et al. Hydrogen production by catalytic methane decomposition: Carbon materials as catalysts or catalyst supports. Int J Hydrogen Energy 2017. https://doi.org/10.1016/j.ijhydene.2017.06.197.

[15] Muradov N. Catalysis of methane decomposition over elemental carbon. Catal Commun 2001;2:89–94. https://doi.org/10.1016/S1566-7367(01)00013-9.

[16] Lee EK, Lee SY, Han GY, Lee BK, Lee TJ, Jun JH, et al. Catalytic decomposition of methane over carbon blacks for CO_2-free hydrogen production. Carbon N Y 2004;42:2641–8. https://doi.org/10.1016/j.carbon.2004.06.003.

[17] Hwan M, Kyoung E, Hyuk J, Jun S, Young G, Kwon B, et al. Hydrogen production by catalytic decomposition of methane over activated carbons : kinetic study. Int J Hydrogen Energy 2004;29:187–93.

[18] Moliner R, Suelves I, Lázaro MJ, Moreno O. Thermocatalytic decomposition of methane over activated carbons: Influence of textural properties and surface chemistry. Int J Hydrogen Energy 2005;30:293–300. https://doi.org/10.1016/j.ijhydene.2004.03.035.

[19] Serrano DP, Botas JA, Pizarro P, Guil-López R, Gómez G. Ordered mesoporous carbons as highly active catalysts for hydrogen production by CH_4 decomposition. Chem Commun 2008:6585–8. https://doi.org/10.1039/b811800k.

[20] Serrano DP, Botas JÁ, Pizarro P, Gómez G. Kinetic and autocatalytic effects during the hydrogen production by methane decomposition over carbonaceous catalysts. Int J Hydrogen Energy 2013;38:5671–83. https://doi.org/10.1016/j.ijhydene.2013.02.112.

[21] Serrano DP, Botas JA, Fierro JLG, Guil-López R, Pizarro P, Gómez G. Hydrogen production

by methane decomposition: Origin of the catalytic activity of carbon materials. Fuel 2010;89:1241–8. https://doi.org/10.1016/j.fuel.2009.11.030.

[22] Botas JA, Serrano DP, Guil-López R, Pizarro P, Gómez G. Methane catalytic decomposition over ordered mesoporous carbons: A promising route for hydrogen production. Int. J. Hydrogen Energy, vol. 35, 2010, p. 9788–94. https://doi.org/10.1016/j.ijhydene.2009.10.031.

[23] Shilapuram V, Ozalp N, Oschatz M, Borchardt L, Kaskel S. Hydrogen production from catalytic decomposition of methane over ordered mesoporous carbons (CMK-3) and carbide-derived carbon (DUT-19). Carbon N Y 2014;67:377–89.

[24] Zhang J, Jin L, Li Y, Hu H. Ni doped carbons for hydrogen production by catalytic methane decomposition. Int J Hydrogen Energy 2013;38:3937–47.

[25] Henao W, Cazaña F, Tarifa P, Romeo E, Latorre N, Sebastian V, et al. Selective synthesis of carbon nanotubes by catalytic decomposition of methane using Co-Cu/cellulose derived carbon catalysts: A comprehensive kinetic study. Chem Eng J 2021;404:126103. https://doi.org/10.1016/j.cej.2020.126103.

[26] Wilfrid B, Slater E. The influence of different surfaces on the decomposition of methane. J Chem Soc Trans 1916;109:160–4. https://doi.org/10.1039/CT9160900160.

[27] Holliday, G.C., Gooderham WJ. The thermal decomposition of methane. Part II. The homogeneous reaction. J Chem Soc 1931:1594–604. https://doi.org/10.1039/JR9310001594.

[28] Holliday, G.C., Exell HC. The thermal decomposition of methane. Part I. Decomposition in silica bulbs. J Chem Soc 1929:1066–74. https://doi.org/10.1039/JR9290001066.

[29] Serrano DP, Botas JA, Pizarro P, Moreno I, Gómez G. Hydrogen production through catalytic methane decomposition promoted by pure silica materials. Int J Hydrogen Energy 2015;40:5237–43.

[30] Gómez G, Botas JÁ, Serrano DP, Pizarro P. Hydrogen production by methane decomposition over pure silica SBA-15 materials. Catal Today 2016;277:152–60.

[31] Yang L, Liu F, He J. Natural sand as a non-conventional catalyst for hydrogen production by methane thermo-catalytic decomposition. Int J Hydrogen Energy 2019;44:11625–33. https://doi.org/10.1016/J.IJHYDENE.2019.03.163.

[32] Genieva SD, Turmanova SC, Dimitrova AS, Vlaev LT. Characterization of rice husks and the products of its thermal degradation in air or nitrogen atmosphere. J Therm Anal Calorim 2008;93:387–96. https://doi.org/10.1007/s10973-007-8429-5.

[33] Selva Priya A, Sunaja Devi KR. Designing Biomass Rice Husk Silica as an Efficient Catalyst for the Synthesis of Biofuel Additive n-Butyl Levulinate. Bioenergy Res 2020. https://doi.org/10.1007/s12155-020-10128-5.

[34] Shen Y, Zhao P, Shao Q. Porous silica and carbon derived materials from rice husk pyrolysis char. Microporous Mesoporous Mater 2014;188:46–76.

[35] Adam F, Appaturi JN, Iqbal A. The utilization of rice husk silica as a catalyst: Review and recent progress. Catal Today 2012;190:2–14.

[36] Liu D, Seeburg D, Kreft S, Bindig R, Hartmann I, Schneider D, et al. Rice husk derived porous silica as support for pd and CeO_2 for low temperature catalytic methane combustion. Catalysts 2019;9:26. https://doi.org/10.3390/catal9010026.

[37] Awadallah AE, Solyman SM, Aboul-Enein AA, Ahmed HA, Aboul-Gheit NAK, Hassan SA. Effect of combining Al, Mg, Ce or La oxides to extracted rice husk nanosilica on the catalytic performance of NiO during CO_x-free hydrogen production via methane decomposition. Int J Hydrogen Energy 2017;42:9858–72. https://doi.org/10.1016/j.ijhydene.2017.03.049.

[38] Obernberger I, Biedermann F, Widmann W, Riedl R. Concentrations of inorganic elements in biomass fuels and recovery in the different ash fractions. Biomass and Bioenergy 1997;12:211–24. https://doi.org/10.1016/S0961-9534(96)00051-7.

[39] Chen H, Chen H. Chemical Composition and Structure of Natural Lignocellulose. Biotechnol. Lignocellul., 2014. https://doi.org/10.1007/978-94-007-6898-7_2.

[40] Mansaray K, Ghaly A. Thermal degradation of rice husks in nitrogen atmosphere. Bioresour Technol 1998;65:13–20. https://doi.org/10.1016/S0960-8524(98)00031-5.

[41] Abbas Q, Liu G, Yousaf B, Ali MU, Ullah H, Munir MAM, et al. Contrasting effects of operating conditions and biomass particle size on bulk characteristics and surface chemistry of rice husk derived-biochars. J Anal Appl Pyrolysis 2018;134:281–92. https://doi.org/10.1016/j.jaap.2018.06.018.

[42] Guerrero M, Ruiz MP, Millera Á, Alzueta MU, Bilbao R. Characterization of Biomass Chars Formed under Different Devolatilization Conditions: Differences between Rice Husk and Eucalyptus. Energy & Fuels 2008;22:1275–84. https://doi.org/10.1021/ef7005589.

[43] Aslam U, Ramzan N, Iqbal T, Kazmi M, Ikhlaq A. Effect of demineralization on the physiochemical structure and thermal degradation of acid treated indigenous rice husk. Polish J Chem Technol 2016;18:117–21. https://doi.org/10.1515/pjct-2016-0057.

[44] Versan Kok M, Özgür E. Thermal analysis and kinetics of biomass samples. Fuel Process Technol 2013;106:739–43. https://doi.org/10.1016/j.fuproc.2012.10.010.

[45] Lee JH, Kwon JH, Lee J-W, Lee H, Chang JH, Sang B-I. Preparation of high purity silica originated from rice husks by chemically removing metallic impurities. J Ind Eng Chem 2017;50:79–85. https://doi.org/10.1016/j.jiec.2017.01.033.

[46] Sing KSW. Reporting physisorption data for gas/solid systems with special reference to the determination of surface area and porosity. Pure Appl Chem 2007;57:603–19. https://doi.org/10.1351/pac198557040603.

[47] Thommes M, Kaneko K, Neimark A V., Olivier JP, Rodriguez-Reinoso F, Rouquerol J, et al. Physisorption of gases, with special reference to the evaluation of surface area and pore size distribution (IUPAC Technical Report). Pure Appl Chem 2015;87:1051–69. https://doi.org/10.1515/pac-2014-1117.

[48] Alemdar A, Sain M. Isolation and characterization of nanofibers from agricultural residues – Wheat straw and soy hulls. Bioresour Technol 2008;99:1664–71. https://doi.org/10.1016/J.BIORTECH.2007.04.029.

[49] Pérez J, Muñoz-Dorado J, De La Rubia T, Martínez J. Biodegradation and biological treatments of cellulose, hemicellulose and lignin: An overview. Int Microbiol 2002;5:53–63. https://doi.org/10.1007/s10123-002-0062-3.

[50] Mašek O, Budarin V, Gronnow M, Crombie K, Brownsort P, Fitzpatrick E, et al. Microwave and slow pyrolysis biochar—Comparison of physical and functional properties. J Anal Appl Pyrolysis 2013;100:41–8. https://doi.org/10.1016/J.JAAP.2012.11.015.

[51] Fernandes IJ, Calheiro D, Kieling AG, Moraes CAM, Rocha TLAC, Brehm FA, et al.

Characterization of rice husk ash produced using different biomass combustion techniques for energy. Fuel 2016;165.

[52] Venezia AM, La Parola V, Longo A, Martorana A. Effect of Alkali Ions on the Amorphous to Crystalline Phase Transition of Silica. J Solid State Chem 2001;161:373–8. https://doi.org/10.1006/JSSC.2001.9345.

[53] Gu S, Zhou J, Luo Z, Wang Q, Ni M. A detailed study of the effects of pyrolysis temperature and feedstock particle size on the preparation of nanosilica from rice husk. Ind Crops Prod 2013;50:540–9. https://doi.org/10.1016/j.indcrop.2013.08.004.

Figure captions

Figure 1. Main inorganic components contained in the raw rice husk samples, expressed as the corresponding oxides.

Figure 2. TG/DTG curves corresponding to the pyrolysis (N_2) of rice husk (a,b) and the combustion (air) of the so-derived char samples (c,d).

Figure 3. (a) N_2 adsorption-desorption isotherms (77 K) and (b) BJH pore size distribution of rice husk derived-silica samples.

Figure 4. X-ray diffractograms: (a) raw and acid-washed rice husk, (b) rice husk derived-char and (c) rice husk derived-silica.

Figure 5. TEM images: a) SiO_2/100 and b) aw-SiO_2/100.

Figure 6. Temperature programmed $DeCH_4$ reaction over different rice husk derived-silica samples.

Figure 7. $DeCH_4$ reaction over the different rice husk derived-silica samples at 965 ºC: a) weight increase of the samples, b) induction time versus BET surface area, c) carbon production at 12 h of time on stream versus BET surface area.

Figure 8. TEM images of the aw-SiO_2/100 sample after being used in $DeCH_4$ at 965 ºC for 12 h.

Figure 9. $DeCH_4$ reaction over: (a) aw-SiO_2/100 and (b) aw-SiO_2/250, and evolution of the carbon deposition rates versus time: (c) aw-SiO_2/100 and (d) aw-SiO_2/250 at reaction temperatures in the range of 890-990 ºC

Figure 10. Arrhenius plots of the $DeCH_4$ reaction over silica samples prepared from acid-washed rice husk: a) Reverse of the induction time, b) Carbon production rate.

FIGURE 1

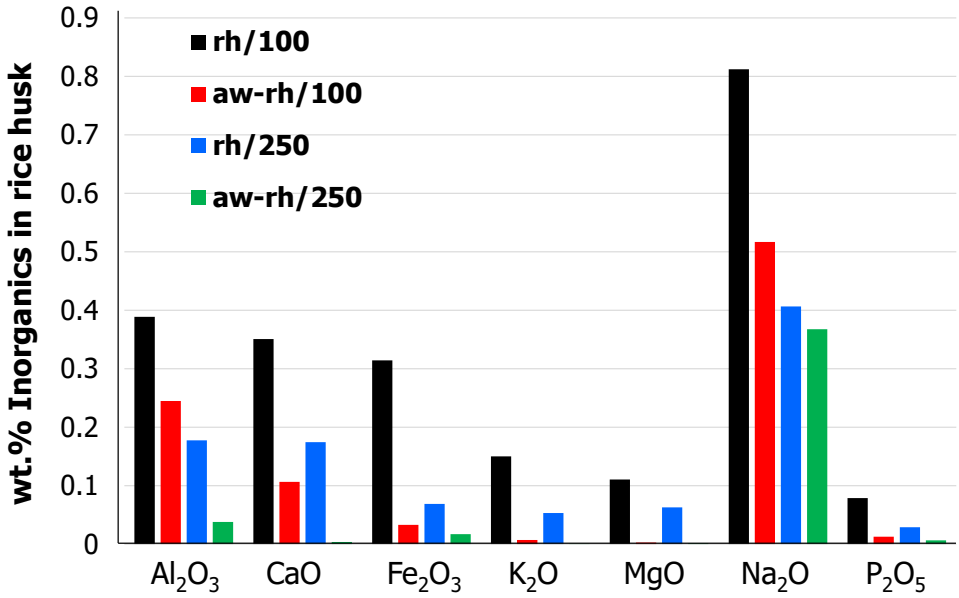

FIGURE 2

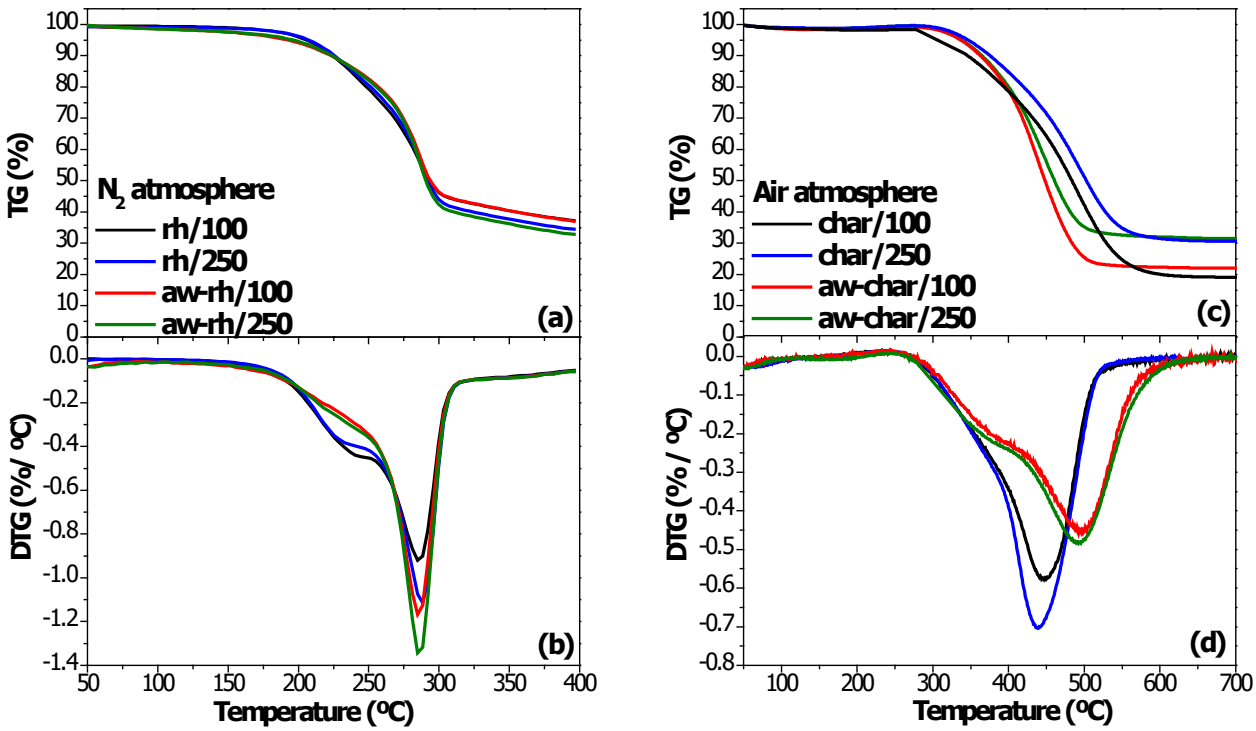

FIGURE 3

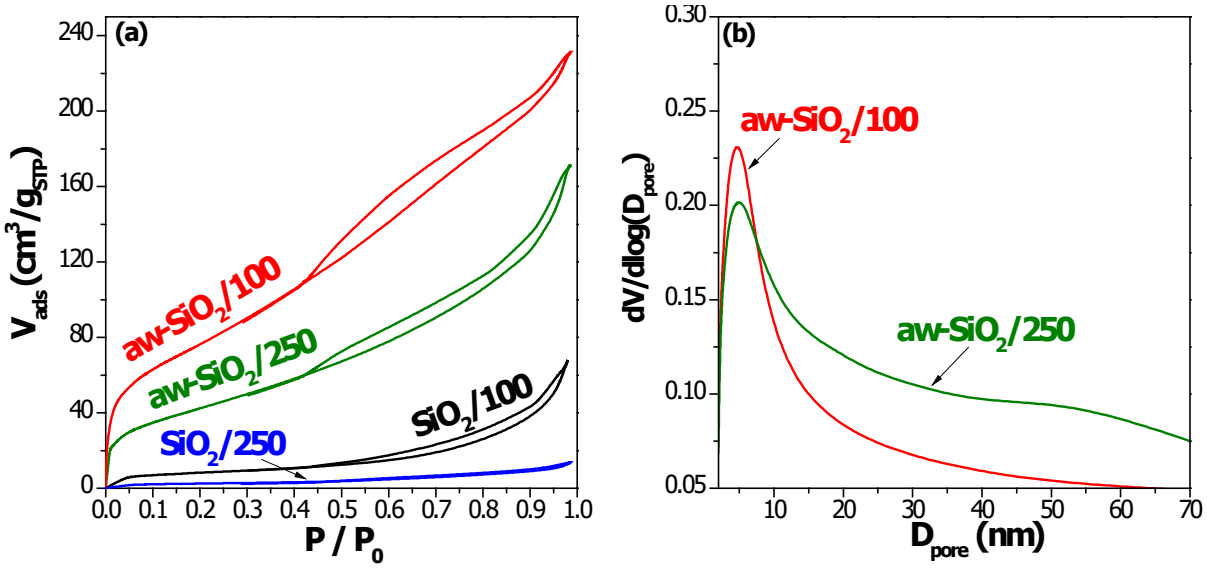

FIGURE 4

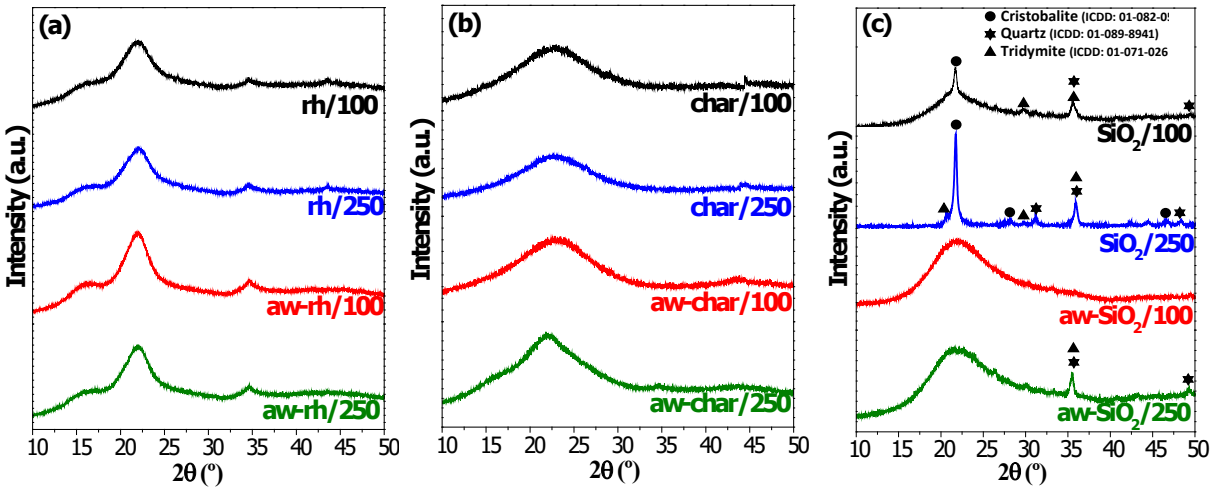

FIGURE 5

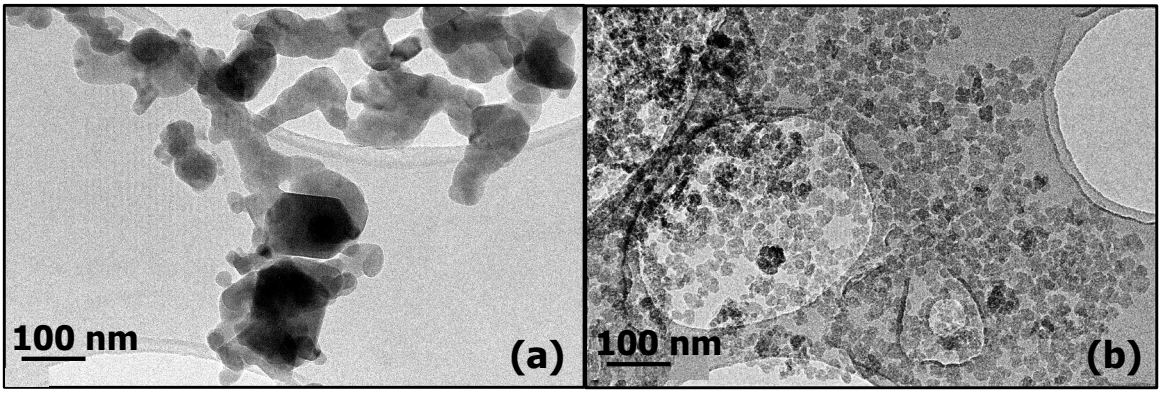

FIGURE 6

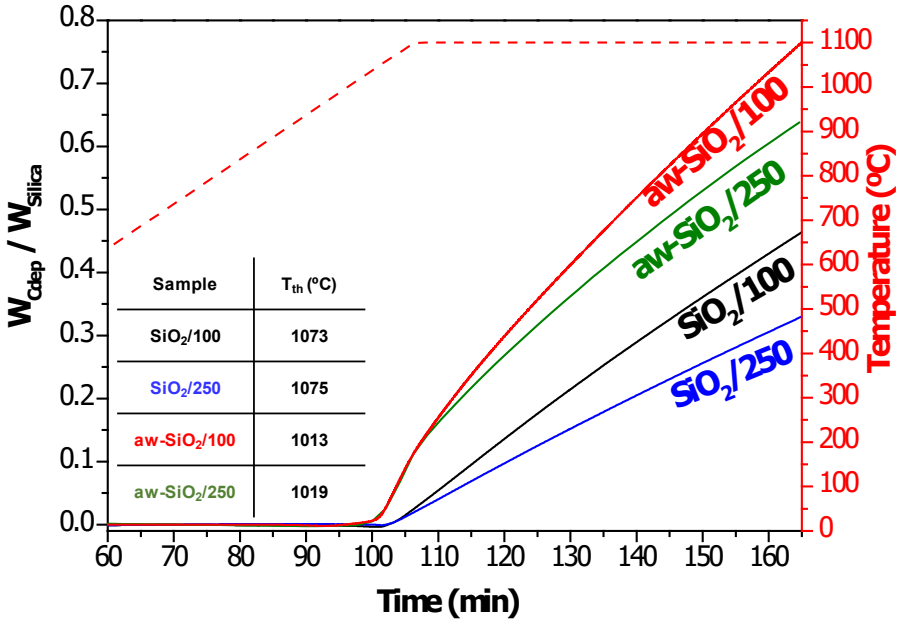

FIGURE 7

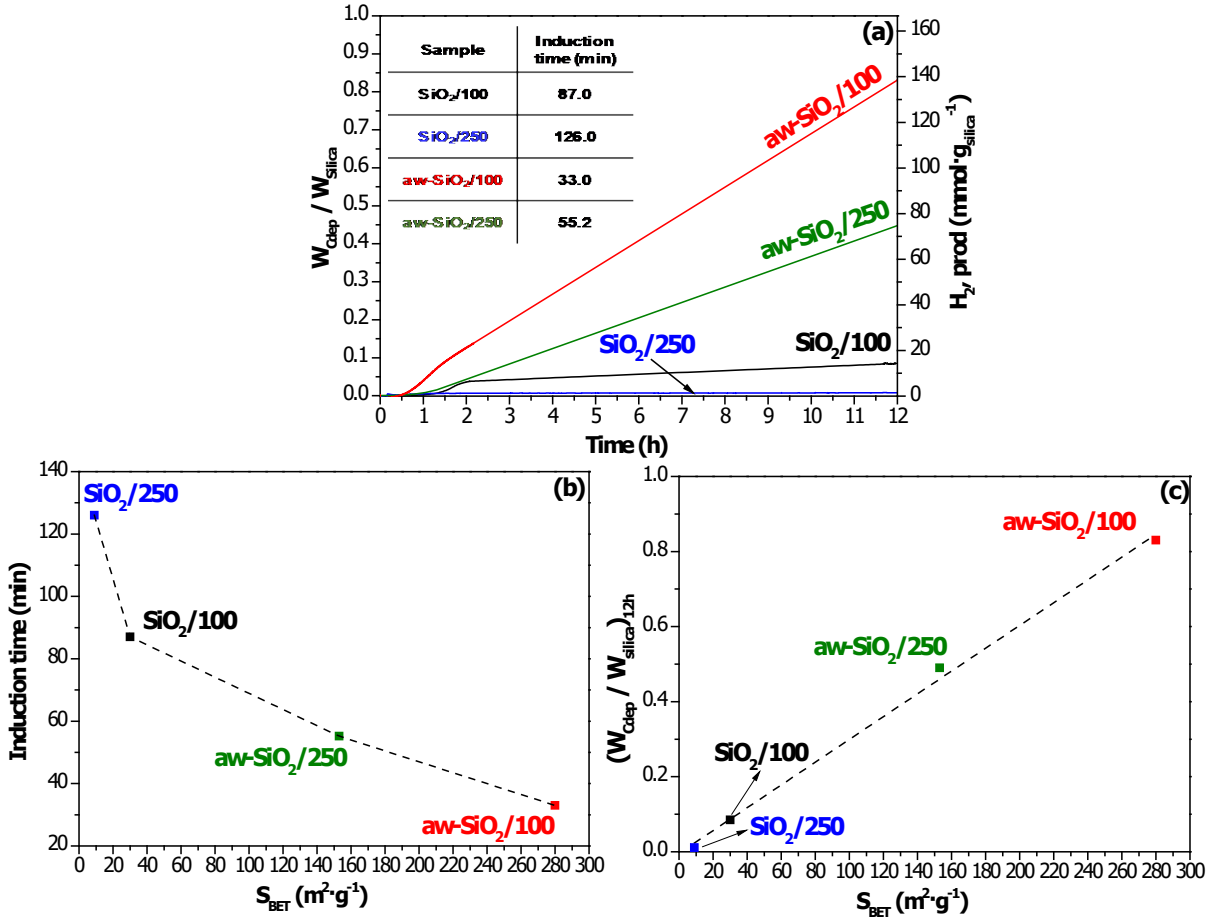

FIGURE 8

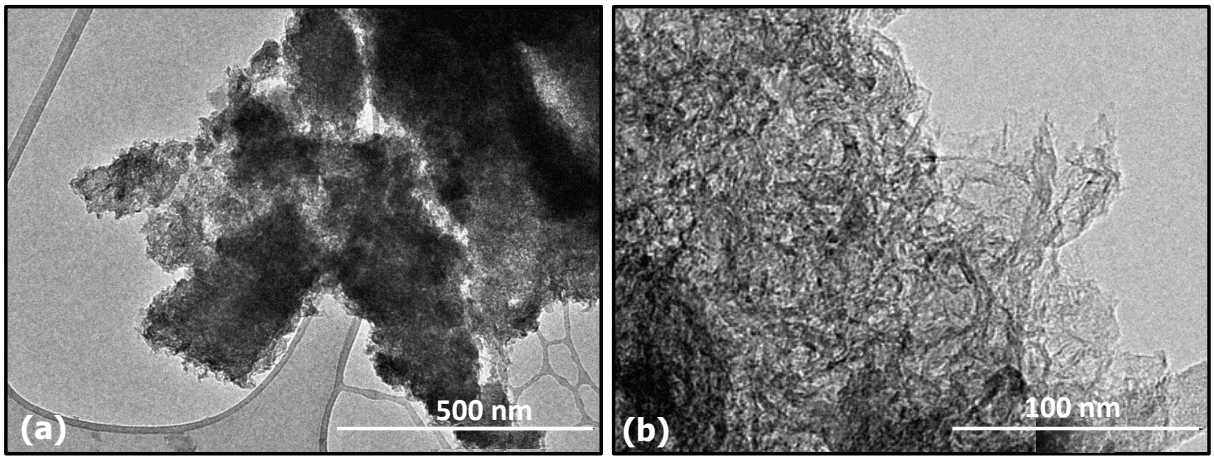

FIGURE 9

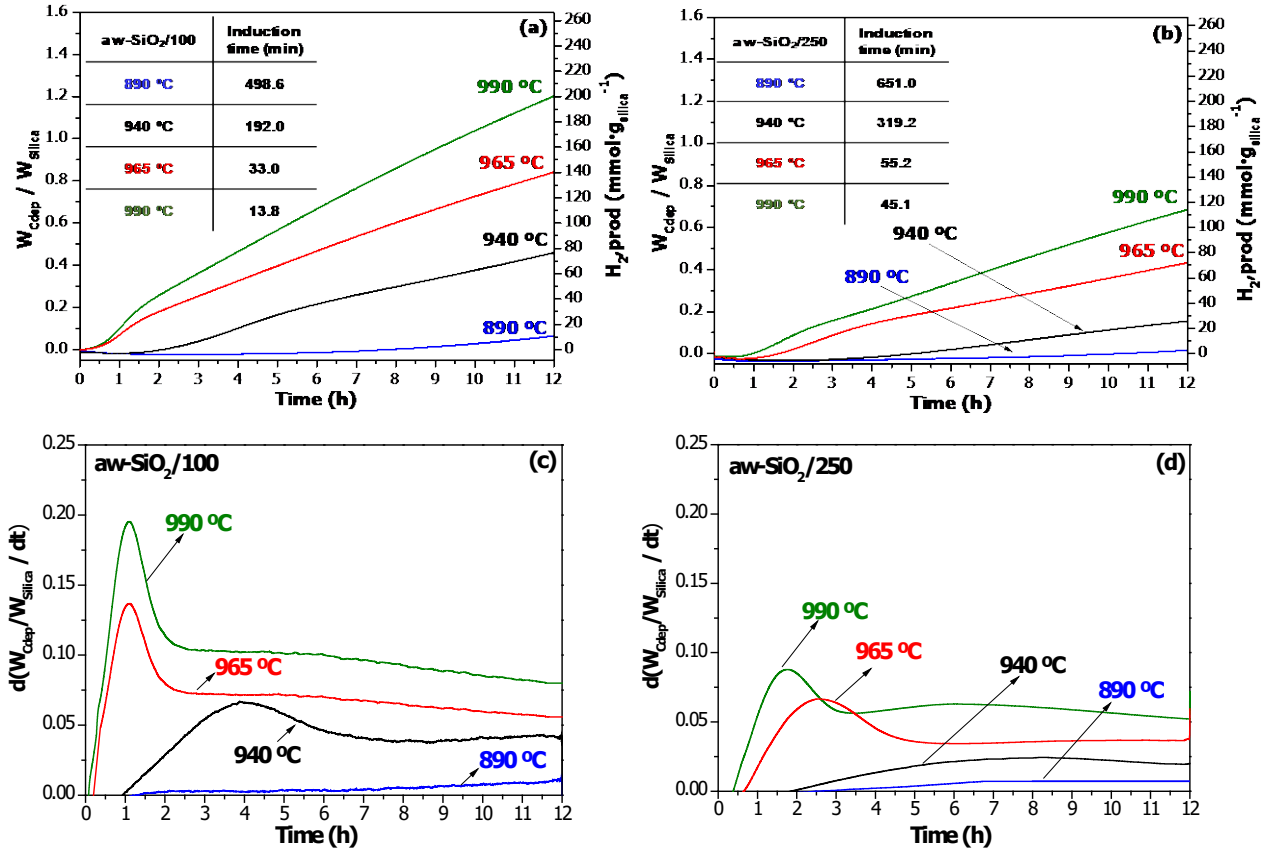

FIGURE 10

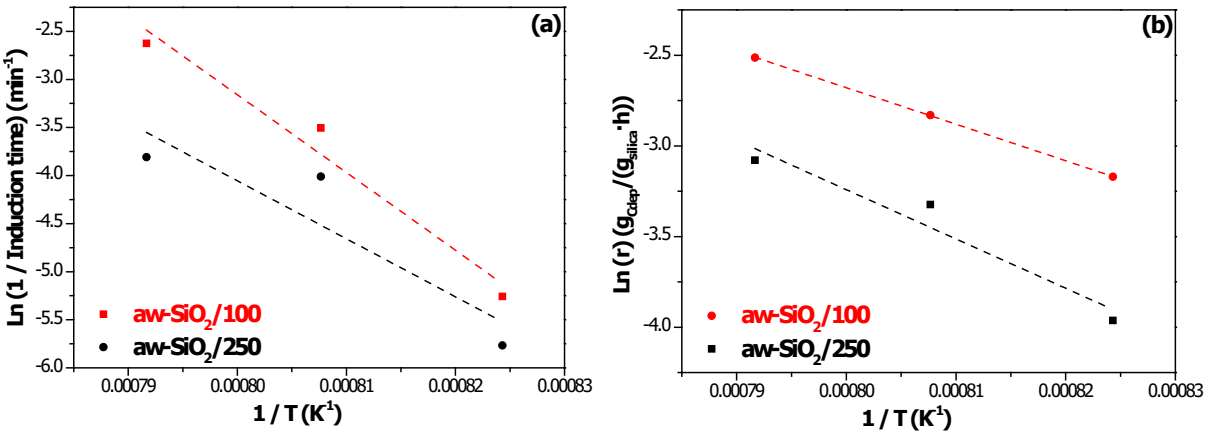
(a)
Ln (1 / Induction time) (min-1)
-2.5
-3.0
-3.5
-4.0
-4.5
-5.0
-5.5
-6.0
aw-SiO2/100
aw-SiO2/250
0.00079
0.00080
0.00081
0.00082
0.00083
1 / T (K-1)
(b)
Ln (r) (gCdep/(gsilica·h))
-2.5
-3.0
-3.5
-4.0
aw-SiO2/100
aw-SiO2/250
0.00079
0.00080
0.00081
0.00082
0.00083
1 / T (K-1)